Supporting Information for *Acta Phys. -Chim. Sin.* doi: 10.3866/PKU.WHXB202012091

高结构稳定性、低泄漏率三维铜@石墨烯复合相变材料的制备

李晓明[1]，高逸丹[1]，孔庆强[1]，谢莉婧[1]，刘卓[1]，郭晓倩[1]，刘燕珍[1]，卫贤贤[3]，杨晓[1]，张兴华[1]，陈成猛[1,2,*]

[1] 中国科学院山西煤炭化学研究所，中国科学院炭材料重点实验室，太原 030001

[2] 中国科学院大学材料科学与光电技术学院，北京 100049

[3] 太原科技大学环境与安全学院，太原 030024

Fabrication of Three-Dimensional Copper@Graphene Phase Change Composite with High Structure Stability and Low Leakage Rate

Xiaoming Li[1,†], Yidan Gao[1,†], Qingqiang Kong[1], Lijing Xie[1], Zhuo liu[1], Xiaoqian Guo[1], Yanzhen Liu[1], Xianxian Wei[3], Xiao Yang[1], Xinghua Zhang[1], Chengmeng Chen[1,2,*]

[1] Key Laboratory of Carbon Materials, Institute of Coal Chemistry, Chinese Academy of Sciences, Taiyuan 030001, China.

[2] College of Materials Sciences and Opto-Electronic Technology, University of Chinese Academy of Sciences, Beijing 100049, China.

[3] College of Environment and Safety, Taiyuan University of Science and Technology, Taiyuan 030024, China.

[*]Corresponding author. Email: ccm@sxicc.ac.cn; Tel.: +86-351-404-9061..

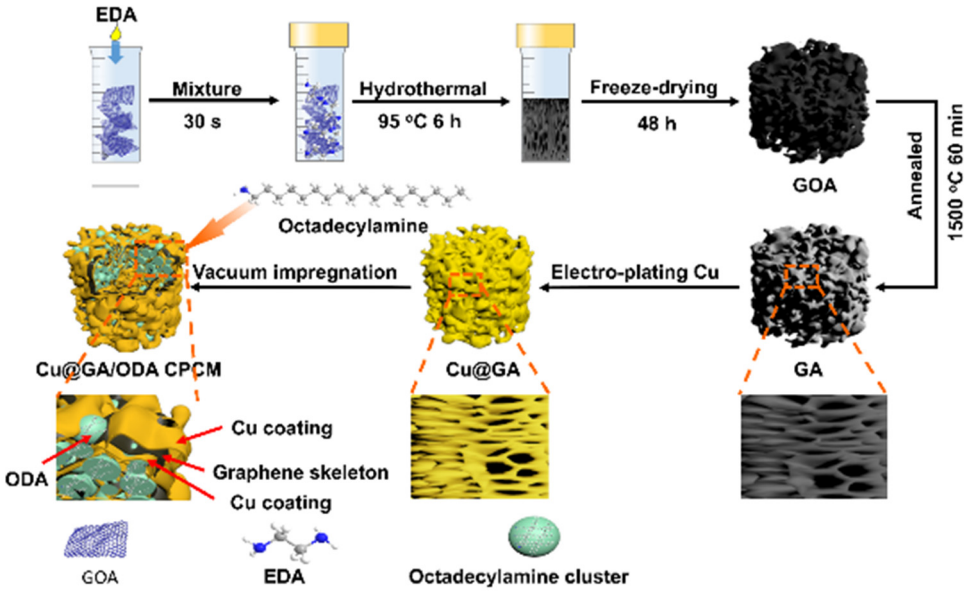

图 S1　GOA, GA, Cu@GA-n and CPCMs 材料的制备流程示意图

Fig. S1　Schematic procedure for the synthesis of GOA, GA, Cu@GA-n and CPCMs.

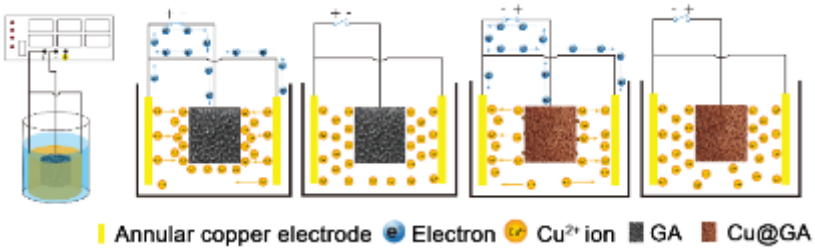

图 S2　双脉冲电源电镀机理示意图

Fig. S2　Schematic of electroplating by double pulse electroplating power.

In the positive impulse mode, lots of cupric ions were concentrated on the cathode region (vicinity of graphene aerogel). The cathode donate electron for the cathodic reduction of cupric ions, which benefits the formation of copper nanoparticles on the surface of GA. After a while, the positive current was switched off, and the concentration of cupric ions recovers to the initial concentration. Meanwhile the polarization concentration and solution resistance were reduced. This would be conducive to next pulse period with higher peak current densities. In this stage, forward current is intermittent rather than persistent. The electrode reaction mechanism follows the half-equation:

Cathode: $Cu^{2+}(aq) + 2e^{-} \rightarrow Cu(s)$ (1)

Anode: $Cu(s) - 2e^{-} \rightarrow Cu^{2+}(aq)$ (2)

After a group of positive impulse, under the action of short time inverse impulse, the bulge of the coated sample would redissolve. Furthermore, the concentration of cupric ions near anode region increased largely, and the surface of sample became smooth and fresh. Thus, the copper particles intermixed and filled reciprocally, and then formed coating layer on the GA surface.

The detailed information about the macroscopic shape-stability and leakage rate test.

The shape-stability of pure ODA and CPCMs is an important aspect for performance reliability during phase change. The poor shape-stability properties can cause PCM leakage, and thereby reducing the energy storage density of the CPCMs. For testing the shape-stability, the samples pure ODA and CPCMs were place on the filter papers and heated at a rate of 5 °C·min^{-1} from 20 to 70 °C. A digital camera was used to record the macroscopic shape-stability of the samples after they were kept at a series temperature (20, 40, 60, 80 °C) for 30 min. It is similar approach as reported by Yang e*t al.* [40]. In addition, the mass change of pure ODA and CPCMs were before and after heating at 80 °C (above the melting point of ODA) for 30 min was used to evaluate the leakage rate (*LR*). Firstly, the samples of known mass (m_0) were put in filter papers. Then, they were moved in a thermostatic oven at 80 °C and kept for 30 min. After the time is up, the sample is removed, weighed and marked as m_1. Repeat the above steps after the sample cools. The mass of samples was labeled as m_i, after each heated in the oven for i times. The leakage rate is calculated by the following Eq. (1):

$$LR_i = (m_0 - m_i)/m_0 \quad (3)$$

i: the number of heated in oven, *i* = 1–20.

This similar method was reported by Zhao *et al*. [41] and Tian *et al*. [42].

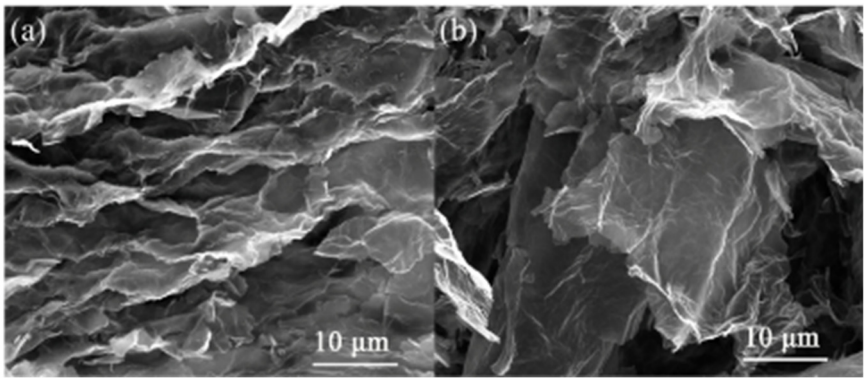

图 S3　(a) GOA 和(b) GA 的扫描电镜图

Fig. S3　SEM images of (a) GOA and (b) GA.

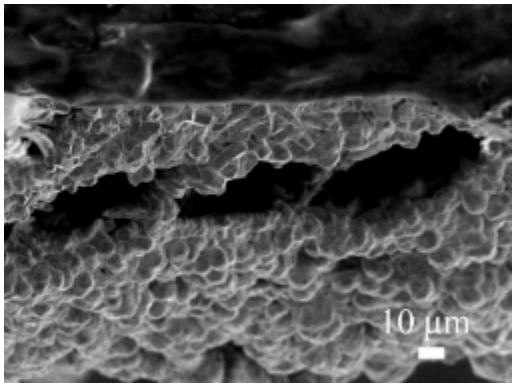

图 S4　Cu@GA40 样品截面扫描电镜图

Fig. S4　Cross-sectional views of Cu@GA40.

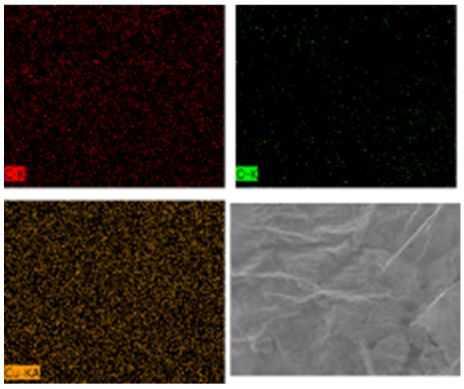

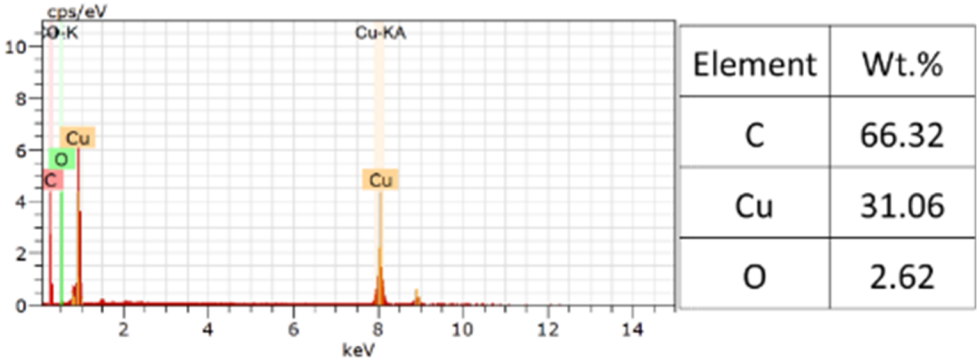

Element	Wt.%
C	66.32
Cu	31.06
O	2.62

图 S5　Cu@GA10 样品的 EDX 面扫元素分布图

Fig. S5　Elemental (C, O, Cu) mapping analysis and EDX spectrum of Cu@GA10.

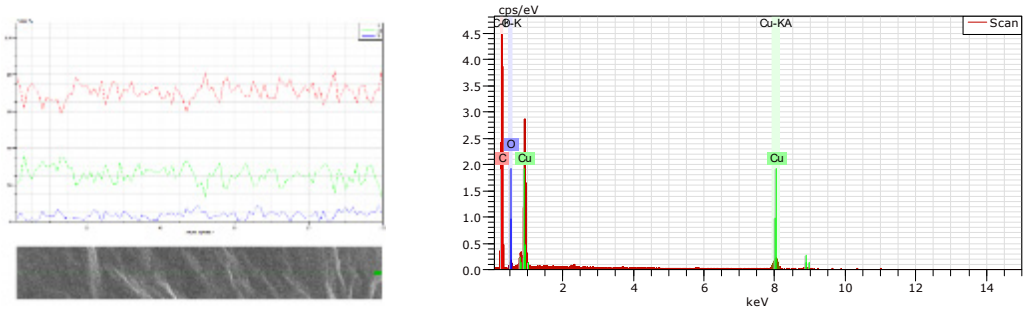

图 S6　Cu@GA10 样品的 EDX 线扫元素分布图

Fig. S6　EDS linescan profile and EDS spectra of Cu@GA10.

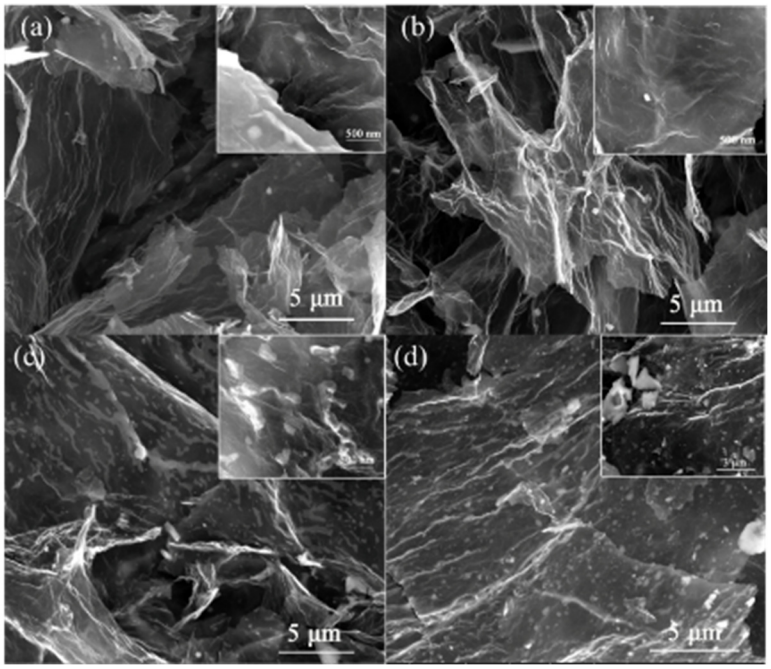

图 S7　不同电镀时间 Cu@GA 复合的扫描电镜图片，(a) 为电镀 10 min，表示为 Cu@GA10，(b) 为电镀 20 min，表示为 Cu@GA20，(c) 为电镀 30 min，表示为 Cu@GA30，(d) 为电镀 40 min，表示为 Cu@GA40

Fig. S7　SEM images of Cu@GAn samples (a) Cu@GA10, (b) Cu@GA20, (c) Cu@GA30 and (d) Cu@GA40.

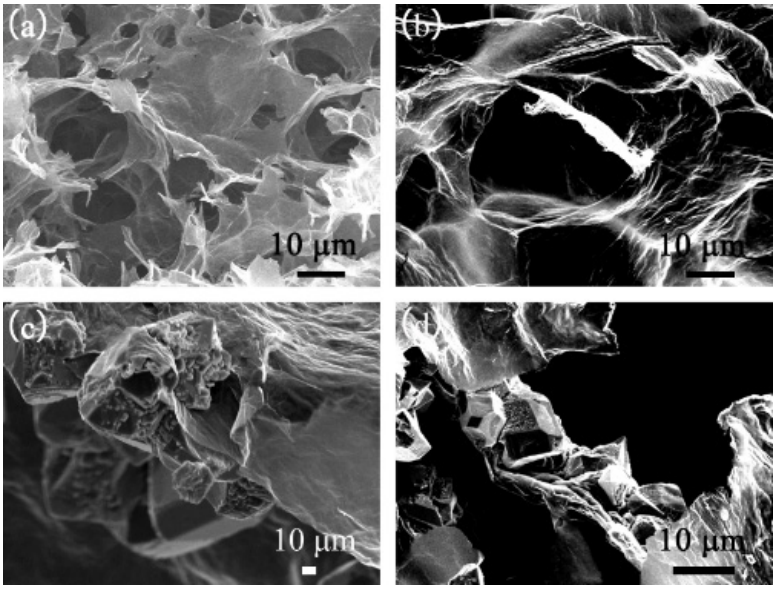

图 S8　(a)为 GA 样品的扫描电镜和(b)–(d)为 Cu@GA40 样品的典型内部结构

Fig. S8　SEM micrographs of (a) GA, (b)–(d) typical inner structures of Cu@GA40.

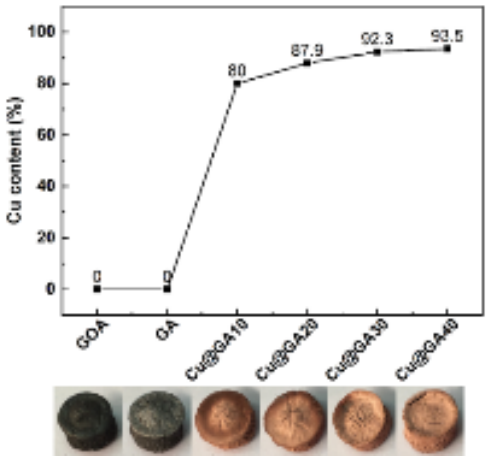

图 S9　GOA, GA and Cu@GAn (Cu content = m_{Cu}/m_{GA})中铜含量随电镀时间的变化曲线

Fig. S9　The variation curves of Cu content of GOA, GA and Cu@GAn (Cu content = m_{Cu}/m_{GA}) at different plating times.

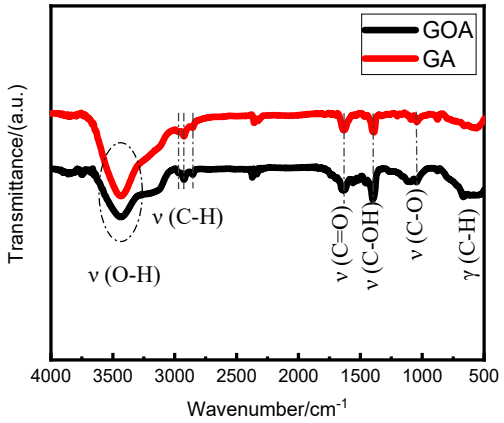

图 S10　GOA 和 GA 的红外光谱曲线

Fig. S10　FT-IR results of GOA and GA.

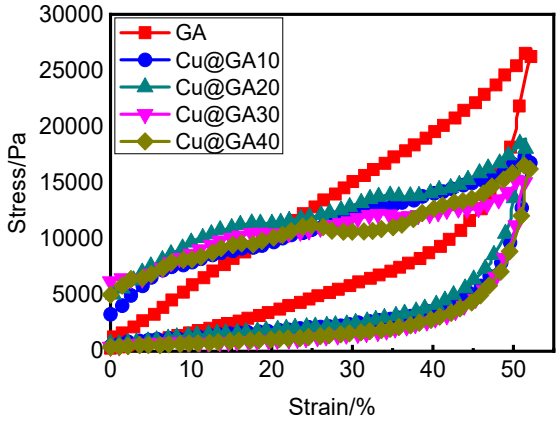

图 S11　GOA, GA and Cu@GA*n* (*n* = 10, 20, 30, 40)在 50%应变范围内的首次应力应变曲线

Fig. S11　The first compressive stress-strain curves of GA and Cu@GA*n* (*n* = 10, 20, 30, 40) within the 50% strain range.

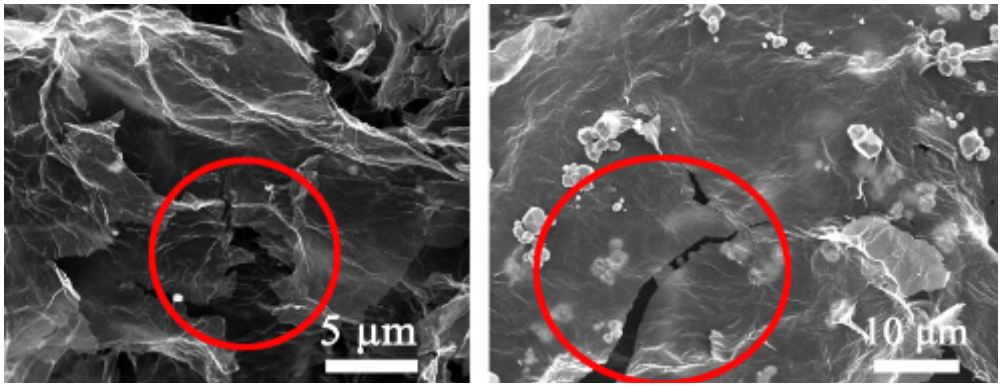

图 S12　Cu@GA10 样品在过载的压力作用下，三维网络结构或石墨烯片遭受破坏

Fig. S12　SEM of Cu@GA10 which under pressure overload, displayed that the three-dimensional net structure and coated copper graphene sheet was destroyed.

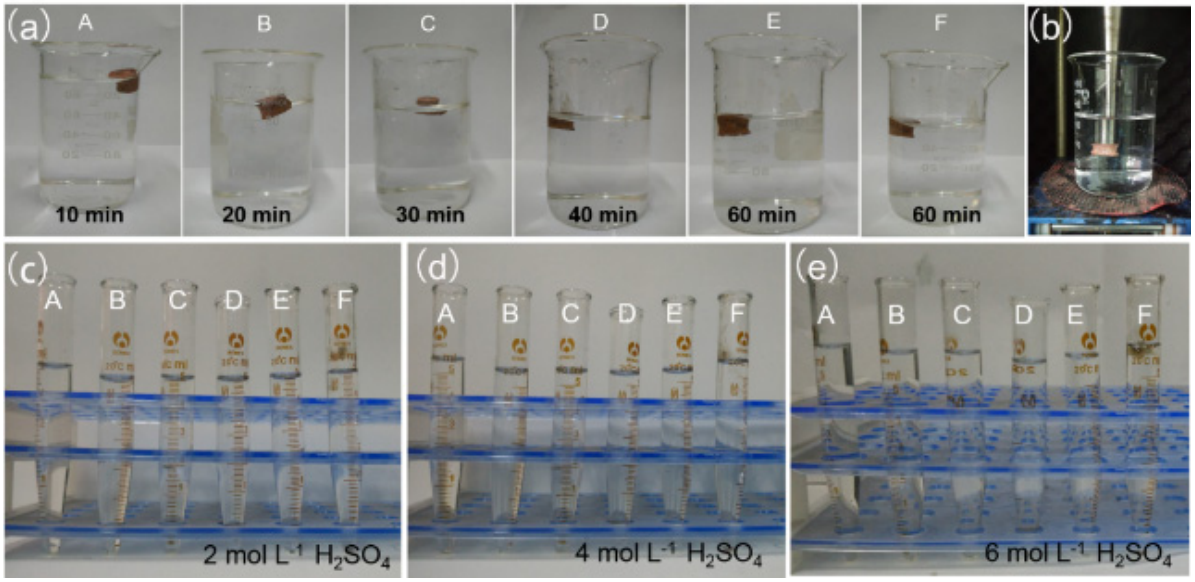

图 S13　用超声波法测试了铜颗粒在石墨烯片表面的附着性能。(a)将 Cu@GA40 浸入去离子水中，然后超声处理不同时间(10–60 min)，(b)为超声检测原理图。结果表明，超声后未在液体中发现铜颗粒或结构碎片。在超声的液体中滴加入过量的(c) 2 mol·L^{-1}, (d) 4 mol·L^{-1}, (e) 6 mol·L^{-1} 硫酸，无明显反应产生

Fig. S13　Adhesion property between copper particles and graphene sheets was test by Ultrasound method. (a) Dip the Cu@GA40 into deionized water, and then ultrasonic treated for different time, (b) Schematic diagram of ultrasonic testing. The results showed that there is no copper particles or fragment of Cu@GA40 after ultrasound. Adding (c) 2 mol·L^{-1}, (d) 4 mol·L^{-1} and (e) 6 mol·L^{-1} vitriol into the fluid after ultrasound, there was still nothing going on.

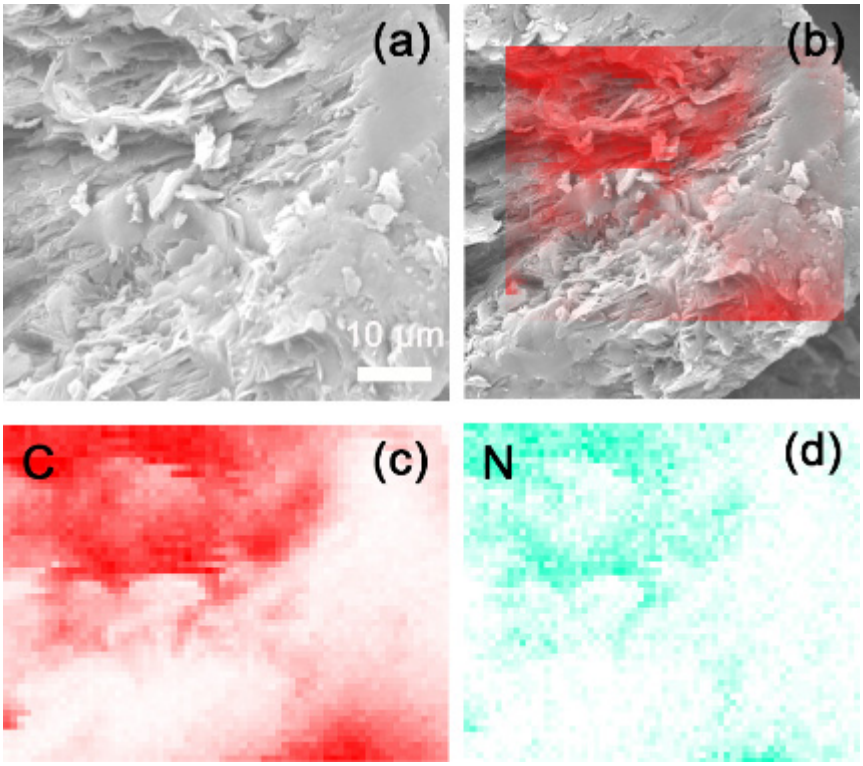

图 S14　Cu@GA/ODA 复合相变材料在相变前的元素分析图谱

Fig. S14　The EDS mapping of Cu@GA/ODA composite before the phase change.

表 S1　Cu@GA/ODA 复合相变材料在相变前的元素占比数据

Table S1　The corresponding EDS element analysis of Cu@GA/ODA composite before the phase change.

Element Number	Element Symbol	Element Name	Atomic Conc./%	Weight Conc./%
6	C	Carbon	83.18	80.92
7	N	Nitrogen	16.82	19.08

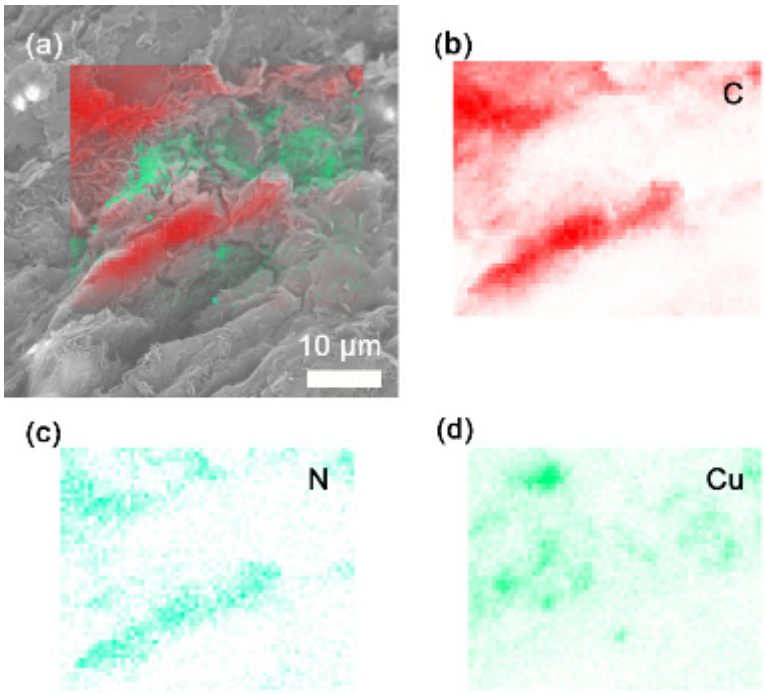

图 S15　Cu@GA/ODA 复合相变材料经过 20 次相变循环后元素分析图谱

Fig. S15　The EDS mapping of Cu@GA/ODA composite after 20 times phase change.

表 S2　Cu@GA/ODA 复合相变材料经过 20 次相变循环后的元素占比数据

Table S2　The corresponding EDS element analysis of Cu@GA/ODA composite after 20 times phase change.

Element Number	Element Symbol	Element Name	Atomic Conc./%	Weight Conc./%
6	C	Carbon	87.92	72.70
7	N	Nitrogen	7.49	7.22
29	Cu	Copper	4.59	20.08

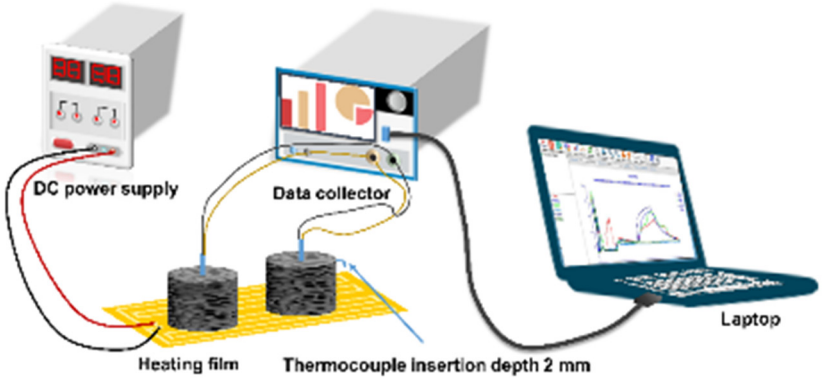

图 S16　复合相变材料热导率和升降温曲线测试装置及示意图

Fig. S16　The device and schematic diagram for measuring the thermal conductivity and the speed of CPCMs temperature-up and temperature-down.

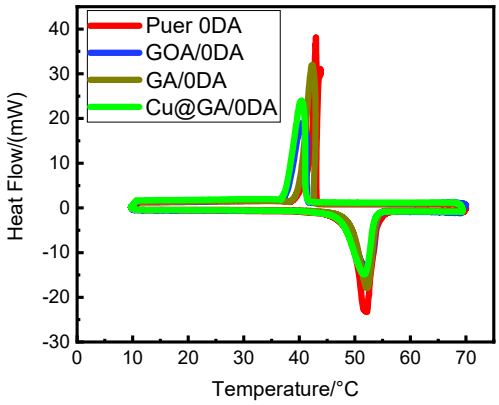

图 S17　纯 ODA, GA/ODA, GA/ODA and Cu@GA/ODA 的 DSC 曲线

Fig. S17　DSC curves of pure ODA, GA/ODA, GA/ODA and Cu@GA/ODA.

表 S3　纯 ODA, GA/ODA, GA/ODA and Cu@GA/ODA 的 DSC 吸热和放热数据

Table S3　DSC heating and cooling data of pure ODA and different composite PCMs.

Sample	T_m/°C	T_c/°C	ΔH_m/(J·g^{-1})	ΔH_c/(J·g^{-1})
Pure ODA	52.17	43.01	264.80	264.60
GOA/ODA	52.01	40.81	250.25	246.05
GA/ODA	52.18	42.33	255.91	250.71
Cu@GA/ODA	51.53	40.63	220.00	218.83

The phase change parameters extracted from DSC curves, such as melting/crystallization temperature (T_m/T_c) and melting/crystallization enthalpy (ΔH_m/ΔH_c) of the composite PCMs, are presented in Table S3.

表 S4　不同相变复合材料的热导率和相变焓损失率

Table S4　The thermal conductivity and the enthalpy loss rate of CPCMs.

No.	Skeleton	Phase change materials	thermal conductivity/($W \cdot m^{-1} \cdot K^{-1}$)	ΔH_m rejection ratio/%	ΔH_c rejection ratio/%	Ref.
1	GO/BN	paraffin	1.84	17.85%	17.77%	23
2	SiO_2/GO	D-mannitol	0.72	21.96%	23.51%	53
3	GO/BN	polyethylene glycol	1.06	5.78%	14.16%	25
4	C_{18}-RGO	paraffin		27.57%	28.87%	10
5	GO/BN	paraffin	1.68	21.96%		35
6	GO/G	lauric acid		7.94%	9.15%	54
7	MF/GO	polyethylene glycol	1.32	5.78%	5.98%	5
8	MG	lauric acid	1.037	2.52%	3.27%	26
9	G/CF	paraffin	2.68	8.59%	7.66%	6
10	PPA/GA	polyethylene glycol	0.61	32.54%	31.99%	55
11	GF/HGA	paraffin wax	1.82	11.73%	14.07%	40
12	Cu@GA	ODA		16.92%	17.30%	This work